Chaos
An Interdisciplinary Journal of Nonlinear Science

RESEARCH ARTICLE | SEPTEMBER 15 2023

Topology switching during window thresholding fMRI-based functional networks of patients with major depressive disorder: Consensus network approach

Alexander N. Pisarchik ; Andrey V. Andreev ; Semen A. Kurkin ; Drozdstoy Stoyanov ; Artem A. Badarin ; Rossitsa Paunova ; Alexander E. Hramov

Chaos 33, 093122 (2023)
https://doi.org/10.1063/5.0166148

Topology switching during window thresholding fMRI-based functional networks of patients with major depressive disorder: Consensus network approach

Cite as: Chaos 33, 093122 (2023); doi: 10.1063/5.0166148
Submitted: 3 July 2023 · Accepted: 29 August 2023 ·
Published Online: 15 September 2023

Alexander N. Pisarchik,[1,2,a)] Andrey V. Andreev,[1] Semen A. Kurkin,[1] Drozdstoy Stoyanov,[3] Artem A. Badarin,[1] Rossitsa Paunova,[3] and Alexander E. Hramov[1]

AFFILIATIONS

[1]Baltic Center for Neurotechnology and Artificial Intelligence, Immanuel Kant Baltic Federal University, 14, A. Nevskogo Str., Kaliningrad 236016, Russia
[2]Center for Biomedical Technology, Universidad Politécnica de Madrid, Campus Montegancedo, Pozuelo de Alarcón 28223, Spain
[3]Department of Psychiatry and Medical Psychology, Research Institute, Medical University Plovdiv, 15A Vassil Aprilov Blvd., Plovdiv 4002, Bulgaria

Note: This paper is part of the Focus Issue on Regime switching in coupled nonlinear systems: sources, prediction, and control.
[a)]**Author to whom correspondence should be addressed:** alexander.pisarchik@ctb.upm.es

ABSTRACT

We present a novel method for analyzing brain functional networks using functional magnetic resonance imaging data, which involves utilizing consensus networks. In this study, we compare our approach to a standard group-based method for patients diagnosed with major depressive disorder (MDD) and a healthy control group, taking into account different levels of connectivity. Our findings demonstrate that the consensus network approach uncovers distinct characteristics in network measures and degree distributions when considering connection strengths. In the healthy control group, as connection strengths increase, we observe a transition in the network topology from a combination of scale-free and random topologies to a small-world topology. Conversely, the MDD group exhibits uncertainty in weak connections, while strong connections display small-world properties. In contrast, the group-based approach does not exhibit significant differences in behavior between the two groups. However, it does indicate a transition in topology from a scale-free-like structure to a combination of small-world and scale-free topologies. The use of the consensus network approach also holds immense potential for the classification of MDD patients, as it unveils substantial distinctions between the two groups.

Studying functional networks in the brain provides a powerful approach to investigate brain functions in both normal and pathological states, enabling the exploration of differences between healthy and pathological brains across various properties. In this study, we utilize resting-state functional magnetic resonance imaging (fMRI) data to analyze functional networks in patients diagnosed with major depressive disorder (MDD) and healthy controls. We compare network measures between the two groups at different levels of connectivity by applying window thresholding within a specific range of connection strength. By varying the window from weak to strong connections, we aim to uncover differences in network characteristics. To conduct a comprehensive analysis, we employ two different approaches: (i) a group-based approach involving the analysis of two groups of networks, and (ii) the analysis of consensus networks corresponding to each group. Using the standard approach, we observe a shift in the network topology for both groups as the threshold increased. The topology changes from a scale-free-like network to a combination of small-world and scale-free networks. On the other hand, analyzing the consensus networks reveals distinct behavior in network measures and degree distributions. In the control group, the network topology shifts from a combination

of scale-free and random topologies to a small-world structure as the threshold increased. In contrast, the network topology in the MDD group exhibits uncertainty in weak connections and displays small-world properties in strong connections. The significant differences observed in network measures using the consensus network approach offer promising potential for easier classification of MDD patients. These findings underscore the utility of consensus network analysis in effectively distinguishing between individuals with MDD and healthy individuals.

I. INTRODUCTION

Analyzing functional networks derived from fMRI data offers significant opportunities for comprehending the intricacies of brain processes in both normal and pathological states.[1,2] Various measures of connectivity can be employed to reconstruct functional networks from fMRI data, with the most commonly used ones being the Pearson correlation coefficient, wavelet correlation, and partial correlation.[3,4] Regardless of the specific measure utilized, the connectivity matrix of the brain typically encompasses a broad spectrum of connectivity levels, ranging from weak to strong. Notably, stronger connections do not necessarily equate to greater significance. In fact, many psychiatric disorders manifest as subtle deviations from the norm in functional connections across multiple levels.[3,5–8]

To address the complexity of brain networks, it is common to binarize connectivity matrices by applying a threshold, considering connections above this threshold as significant, and studying the resulting sparse networks.[9] However, choosing the appropriate threshold value can be challenging in the absence of a complete understanding of network properties.[10] Another approach that can be employed is filtration, which captures the outcomes of all possible binarizations of the network along with their associated threshold values.[9] The resulting dependencies contain valuable information regarding changes in network characteristics. For instance, sudden transitions in network structure as the threshold value varies can indicate regime switching. Consequently, filtration offers a more powerful, sophisticated, and less commonly utilized approach to studying brain networks.

In this paper, we introduce an advanced extension of the filtration approach termed "window thresholding." This approach enables the identification of a characteristic sub-network whose connection strengths fall within a specific range. By shifting this window from smaller to larger values, we can analyze the transformation or switching of sub-networks associated with different scales of connections. Window thresholding offers a comprehensive analysis of the intricate structure of brain networks, facilitating the identification of network components across various levels of connection strengths.

In this study, we employ the proposed approach for the first time to the best of our knowledge to investigate differences in functional networks derived from resting-state fMRI data between healthy individuals and patients diagnosed with major depressive disorder (MDD). MDD is a prevalent psychiatric disorder worldwide and is associated with significant impairment, morbidity, and mortality. In the field of psychiatry, the diagnostic challenges of MDD stem from the limitations, ambiguity, and subjectivity of traditional clinical assessments and subjective reports.[11] In our analysis, we examine the characteristics of functional networks by exploring the transformations in their topologies as the thresholding window is adjusted.

The observed differences between the MDD and healthy control (HC) groups in our study are regarded as potential biomarkers for the diagnosis of MDD. Recent research has highlighted the impact of conventional thresholding on the distinctions between functional networks in MDD patients and healthy individuals.[8,12] Pitsik *et al.*[12] utilized a graph neural network (GNN) to classify MDD by leveraging the topological attributes extracted from brain functional connectivity data obtained through fMRI technology. Their study underscores the significance of the shortest path as a pivotal feature within the functional brain network. This characteristic dictates the optimal number of GNN layers essential for achieving highest classification accuracy for MDD patients, contingent on the chosen threshold value. Nevertheless, the ranges of connection strengths where these differences are most prominent remain unclear due to the limitations of conventional thresholding in addressing this question. The present study aims to fill this gap by providing insights into these significant ranges of connection strengths.

Addressing high inter-subject variability is a major challenge when analyzing clinical data, including the investigation of functional networks in MDD patients. To mitigate this issue, we utilize the concept of a "consensus network."[13] A consensus network is a representative network comprising connections that are shared among all individuals within a given group. This approach boasts numerous successful applications. Notably, it has been employed in diverse scenarios, such as the construction and examination of brain consensus connectomes,[14] the generation and analysis of consensus networks for inferring potential gene interactions,[15] and the visualization of species phylogenies pertaining to a multitude of independent genes.[16] By employing this approach, we aim to account for individual variations and focus on the commonalities in the functional networks of MDD patients.

Furthermore, we compare the standard group-based approach, which considers the functional networks of all individuals from both the MDD and control groups, with the consensus network approach. This comparison allows us to evaluate the effectiveness and advantages of the consensus network approach in capturing the shared characteristics within each group while accounting for inter-subject variability.

II. METHODS

A schematic representation of the research paradigm and its overall structure is depicted in Fig. 1. This diagram illustrates the impact of the methods applied to the original data. The subsequent sections provide an in-depth explanation of both the data and the methodologies employed.

A. Experimental data

In our study, we utilized a dataset comprising a set of 166×166 symmetric functional connectivity matrices. These matrices were

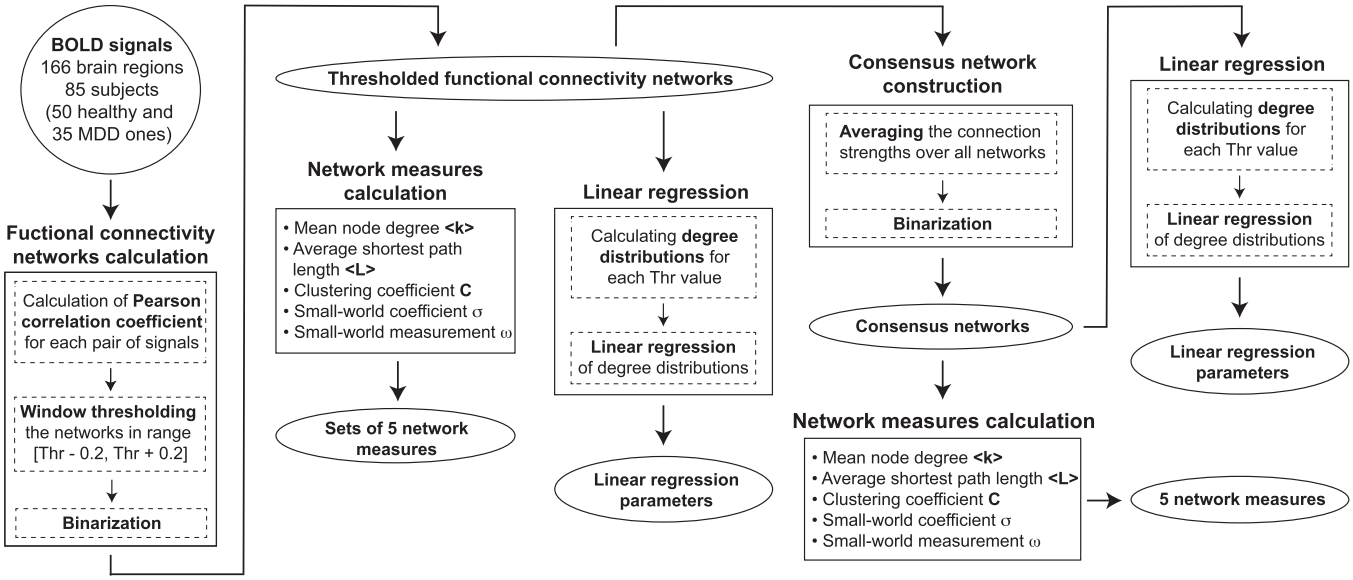

FIG. 1. Schematic depiction of the comprehensive structure. Rectangular frames delineate the successive data analysis steps, while oval frames denote the input/output data associated with each corresponding step.

obtained from blood-oxygen-level dependent (BOLD) signals measured in 166 distinct brain regions. Functional connectivity measures the statistical dependencies and interactions between these regions. The BOLD signal, captured through functional magnetic resonance imaging (fMRI), provides insights into changes in deoxyhemoglobin concentrations, which arise from localized variations in brain blood flow and oxygenation. These changes are associated with underlying neuronal activity, a phenomenon known as neurovascular coupling.

The dataset employed in our analysis consisted of connectivity matrices obtained from 85 subjects by the calculation of Pearson correlation coefficients[4] for resting-state fMRI signals from 166 brain regions. Among these subjects, 50 individuals constituted the healthy control group (HC group), while 35 subjects were diagnosed with major depressive disorder (MDD group). A comprehensive account of the MRI data acquisition and its subsequent progression through standard preprocessing procedures can be found in Sec. 2.1.3 of Ref. 12.

B. Network measures

Each functional connectivity matrix was transformed into a network representation, allowing for the analysis of its structure and topology. We computed several global measures to characterize the network, including the mean node degree $\langle k\rangle$, average shortest path length $\langle L\rangle$, clustering coefficient C, small-world coefficient σ, and small-world measure ω. These measures provide valuable insights into the connectivity patterns and organization of the networks under investigation. Mean node degree is calculated as[17]

$$\langle k\rangle = \frac{1}{N}\sum_{i=1}^{N} k_i, \tag{1}$$

where k_i is the degree of ith node, i.e., the number of edges connected to the ith node, N is the number of nodes in the whole graph.

The average shortest path length is calculated as[18]

$$\langle L\rangle = \frac{\sum_{i=1}^{N}\sum_{j=1}^{N} L_{ij}}{N(N-1)}, \tag{2}$$

where L_{ij} is the shortest path between ith and jth nodes. $L_{ii} = 0$ for $i = 1, \ldots, N$, so we exclude it from consideration.

The Watts–Strogatz clustering coefficient is computed as[19,20]

$$C = \frac{1}{N}\sum_{i=1}^{N} 2n_i/k_i(k_i - 1), \tag{3}$$

where n_i is the number of direct edges interconnecting the k_i nearest neighbors of the ith node.

The small-world coefficient is estimated as[21]

$$\sigma = \frac{C/C_r}{\langle L\rangle/\langle L_r\rangle}, \tag{4}$$

where C_r and $\langle L_r\rangle$ are the clustering coefficient and the average shortest path length for an Erd dos–Rényi random graph with the same number of nodes and edges, respectively. $\sigma > 1$ means the considered network has the properties of the small-world topology.

Finally, the small-world measurement is calculated as[22]

$$\omega = \frac{\langle L_r\rangle}{\langle L\rangle} - \frac{C}{C_l}, \tag{5}$$

where C_l is the clustering coefficient for equivalent lattice network. By evaluating ω, we can determine the degree to which the network exhibits characteristics of a lattice, random, or small-world structure. In particular, $\omega = -1$ corresponds to a lattice network, $\omega = 1$

represents a random network, and $\omega = 0$ indicates a small-world network.

For calculating the network measures, we utilized the open-source NetworkX package in Python. This powerful library provided us with the necessary tools and functions to compute the mean node degree, average shortest path length, clustering coefficient, small-world coefficient, and small-world measure. The NetworkX package offers a user-friendly and efficient framework for analyzing and visualizing complex networks in a Python environment.

C. Window thresholding

The weights of edges, denoted as w, in the fMRI-based functional networks obtained are distributed in the range of 0–1. To analyze specific ranges of edge weights, we introduce a threshold value Thr. By applying a window thresholding technique, we retain the edges with weights within a certain range of $2\Delta Thr$,

$$Thr - \Delta Thr < w < Thr + \Delta Thr. \tag{6}$$

Increasing the threshold value Thr in the network analysis results in retaining only strong connections while disregarding weaker ones. As a consequence, some nodes may become disconnected, indicated by a strength value of 0. In order to maintain a connected network, we remove these disconnected nodes from the analysis. Moreover, if the graph becomes disconnected as a whole, we select the largest connected component for further investigation. After applying the thresholding, the resulting networks are considered unweighted, with all remaining connections assigned a weight of 1. This simplification allows us to focus on the binary presence or absence of connections rather than their specific strengths.

In our empirical analysis, we selected a value of $\Delta Thr = 0.2$ to define the width of the coupling strength window. We then varied the threshold value Thr within the range of [0, 0.8]. This range allowed us to investigate the network properties and transitions within a window width of 0.4 for each considered Thr value. By systematically exploring different threshold values, we were able to analyze the effects of varying connection strengths on the network structure and topology.

D. Linear regression

To approximate the degree distributions, we employed linear regression using the open-source Scikit-Learn package in Python. The degree distributions were analyzed on a double logarithmic scale, allowing us to explore the relationship between the degree and the frequency of nodes. Through linear regression, we obtained the following linear approximation:

$$\log_{10} P^*(k) = \alpha \log_{10} k + \epsilon, \tag{7}$$

where α and ϵ are the angle and constant coefficients, respectively, k is the degree values, $P^*(k)$ is the approximated value.

To assess the quality of the linear approximation, we use the coefficient of determination, also known as the R-squared value. This statistical measure quantifies the proportion of the variance in the data that is captured by the linear regression model. It is defined as

$$R^2 = 1 - \frac{\sum (P(k) - P^*(k))^2}{\sum (P(k) - \bar{P}(k))^2}, \tag{8}$$

where $P(k)$ is the real value, $\bar{P}(k)$ is the mean real value. $R^2 = 1$ indicates that the regression predictions perfectly fit the data.

E. Consensus network

The fundamental concept behind constructing a consensus network is to identify the shared connections observed in the majority of networks within each group (HC and MDD groups). To construct a consensus network, we complete the following procedure for each group:

(1) Thresholding all the networks for a Thr value.
(2) Binarization of all networks, so each connection strength transforms as

$$w_{ij} = \begin{cases} 1 & \text{if } w_{ij} > 0, \\ 0 & \text{if } w_{ij} = 0. \end{cases} \tag{9}$$

(3) Averaging the connection strengths over all networks in the group,

$$w^*_{ij} = \frac{1}{N} \sum_{n=1}^{N} w^n_{ij}, \tag{10}$$

where n is the network number, N is the number of networks in the group.
(4) Binarization of the resulting connection strengths as follows:

$$w^*_{ij} = \begin{cases} 1 & \text{if } w^*_{ij} \geq 0.95, \\ 0 & \text{if } w^*_{ij} < 0.95. \end{cases} \tag{11}$$

The resulting connectivity matrix $\mathbf{w}^*$ corresponds to the consensus network for the considered group.

Figure 2 portrays a schematic overview of the consensus network construction process using an exemplary network. For this illustration, we selected a collection of 20 networks, each featuring 5 nodes interconnected by random undirected connections. The procedure involved computing the average of all connections utilizing Eq. (10), followed by binarization using Eq. (11).

III. RESULTS

To facilitate a thorough investigation of the functional connectivity networks, we employ two distinct approaches: (i) a group-based network analysis applied separately to the HC and MDD groups, and (ii) an analysis of the consensus networks corresponding to each of the HC and MDD groups. By utilizing both approaches, we aim to gain a comprehensive understanding of the network properties and potential differences between the two groups.

A. Group-based network analysis

For each threshold value (Thr), we apply thresholding by retaining only the connections with a strength w within the range defined in Eq. (6). Next, we examine the network properties of the

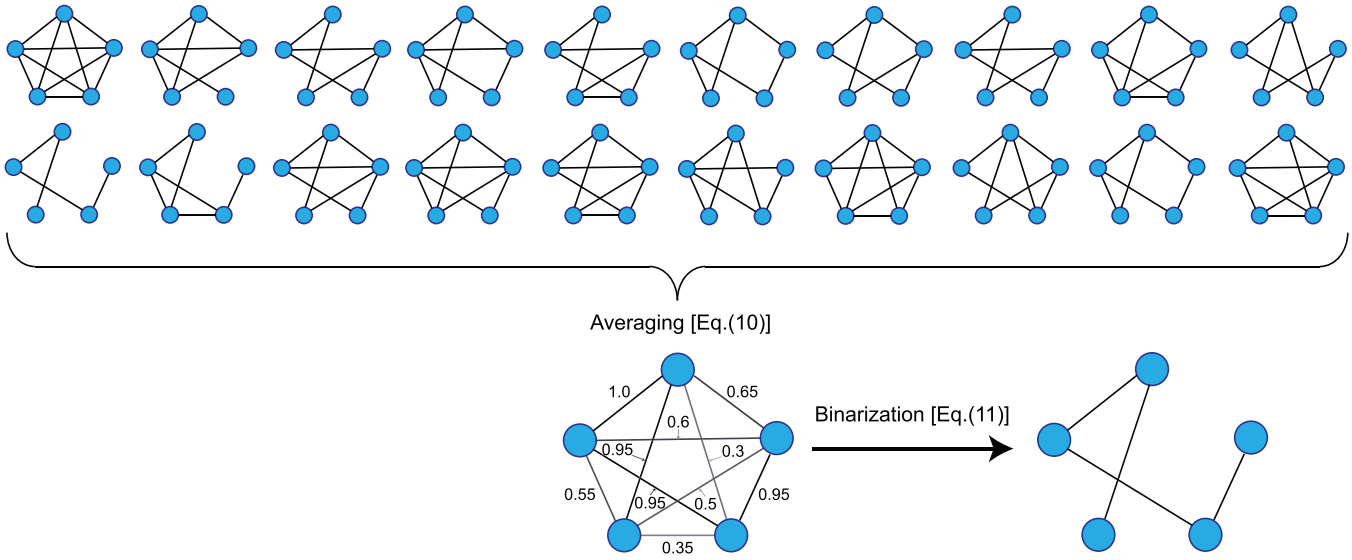

FIG. 2. Schematic representation of the construction of a consensus network using an illustrative example network with five nodes.

HC and MDD groups. We begin by plotting the degree distributions, which are averaged over all the networks for each group, on a log–log scale. Linear regression is applied to estimate the parameters, as shown in Eq. (7). Figure 3 visualizes the degree distributions of networks corresponding to different threshold values *Thr*.

It is noteworthy that the distributions for weak connections with $Thr < 0.3$ can be accurately approximated by linear regression. This indicates a power-law behavior on the linear scales, characterized by an exponent α that is typical of networks with a scale-free topology. As the threshold value *Thr* increases up to 0.4, the distributions become more similar to each other. However, they also exhibit greater nonlinearity in the log–log representation.

A distinct feature is observed at $k = 10^{1.75}$ for the MDD group and at $k = 10^2$ for the HC group, both occurring at $Thr = 0.5$. This peak diminishes as the threshold value increases. Moreover, for high threshold values ($Thr > 0.6$), the distributions resemble heavy-tailed power-law distributions and exhibit increasing similarity among themselves.

To assess the quality and properties of the linear regression, we use the angle α [Eq. (7)] and the coefficient of determination R^2 [Eq. (8)]. Notably, the angle α estimated on a double logarithmic scale corresponds to the exponent α of a power law. Figure 4 displays the dependencies of α and R^2 on the *Thr* value for both groups.

Observing the plots, we can see that as the *Thr* value ranges from 0.2 to 0.6, both the angle of linear regression and the coefficient of determination decrease in absolute values. However, with further increases in the threshold value, their dynamics reverse. It is noteworthy that the HC group exhibits a broader range of variation in these parameters: $\alpha \in [-1.35, -0.25]$ and $R^2 \in [0.1, 0.8]$, compared to the MDD group with $\alpha \in [-0.9, -0.5]$ and $R^2 \in [0.25, 0.55]$.

Figures 3 and 4 provide insights into the degree distributions and angles of linear regression for different threshold values. Notably, for both low (0.2) and high (0.8) threshold values, the distributions (particularly for the HC group) exhibit a strong linear approximation in the log–log scale. Consequently, the network topology can be described as scale-free, characterized by a power-law distribution with an angle of linear approximation in the range of [2, 3].[23]

To explore additional network properties, we calculate several global network measures, including mean node degree $\langle k \rangle$, average shortest path length $\langle L \rangle$, clustering coefficient C, small-world coefficient σ, and small-world measurement ω. Figure 5 depicts the dependencies of these measures on the threshold value *Thr* for both groups. Each line represents the mean value of the measure for the group, while the vertical lines indicate the standard deviation within the group.

Interestingly, node degree and average shortest path exhibit contrasting dynamics as the threshold changes. In the case of the MDD group, these measures show changes within a narrow range of values. Conversely, for the Control group, the measures display significant variations. As the threshold transitions from 0.2 to 0.6, $\langle k \rangle$ increases while $\langle L \rangle$ decreases. However, with a further increase in *Thr*, these changes are reversed.

The clustering coefficient demonstrates an increasing trend across the entire range of threshold values, reaching values of 0.3–0.6 for the HC group and 0.7 for the MDD group. Notably, the clustering coefficient values consistently remain higher for the HC group compared to the MDD group.

The small-world coefficient σ and small-world measurement ω are significant network measures as they characterize the properties of small-world topology in the analyzed networks. Notably, the mean values of σ are consistently greater than 1 for all threshold values in both groups, indicating the presence of small-world properties in the network topology.

However, the small-world measurement ω exhibits interesting behavior. Starting at 0.5 for $Thr = 0.2$, ω decreases to nearly 0 for

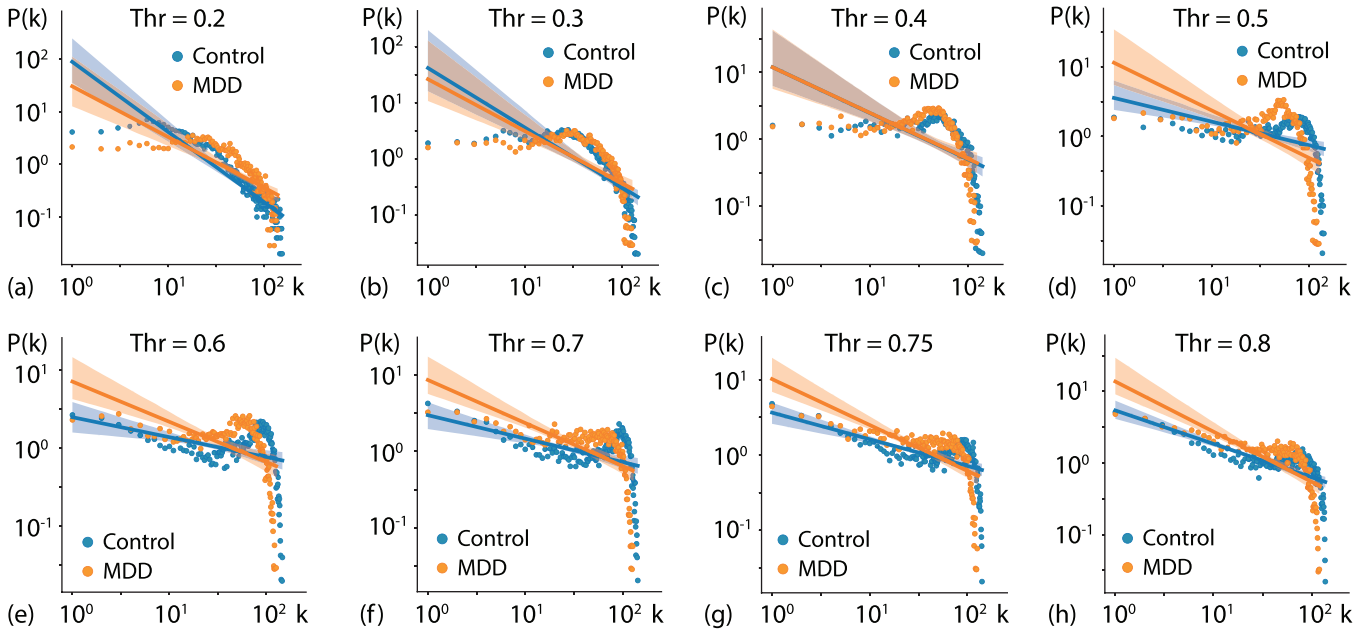

FIG. 3. Degree distributions of networks in a log–log scale corresponding to each threshold value with linear regression: *Thr* = (a) 0.2, (b) 0.3, (c) 0.4, (d) 0.5, (e) 0.6, (f) 0.7, (g) 0.75, (h) 0.8. Each figure shows degree distributions for two groups of subjects (blue—MDD, orange—HC group).

the MDD group and −0.1 for the HC group as the threshold value increases. This suggests that for weak connections, the network topology lies between fully random and small-world topologies. As the threshold value increases, the network topologies of both groups transition toward a small-world topology.

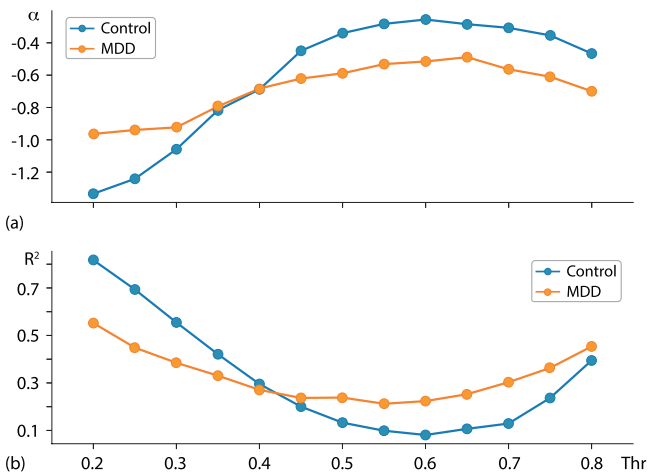

FIG. 4. The dependencies of the linear regression parameters on the threshold value *Thr* for HC (blue) and MDD (red) groups: (a) the angle coefficient α and (b) the coefficient of determination R^2.

Thus, the group analysis of the topological properties of the networks reveals similar behaviors in both healthy control and MDD patients as the threshold value is changed. This similarity poses a challenge when it comes to classifying and analyzing the distinctive features of functional brain network organization in patients using this approach. It suggests that the examined network properties may not be effective discriminators between healthy individuals and those with MDD, highlighting the need for alternative approaches or additional features to improve classification accuracy in this context.

B. Consensus network analysis

As an alternative approach for analyzing the topological properties of functional connectivity networks, we employed the construction and analysis of consensus networks for both the HC and MDD groups. The consensus network was constructed using the mathematical approach described in Sec. II E. Figure 6 presents the degree distributions of the consensus networks on a log–log scale for each threshold value *Thr*, along with linear regression lines for both the HC and MDD groups. Notably, the distributions exhibit notable differences at low *Thr* values, gradually becoming more similar to each other as the threshold value increases.

Figure 7 displays the dependencies of the linear regression parameters, specifically the angle coefficient (α) and the coefficient of determination (R^2), on the threshold value *Thr* for both groups. In the case of the HC group, the linear approximation demonstrates good quality for low threshold values ($R^2 > 0.8$), but its effectiveness decreases as *Thr* increases. The angle coefficient shows a gradual decrease in absolute values, ranging from −1.4 to −0.4. Conversely,

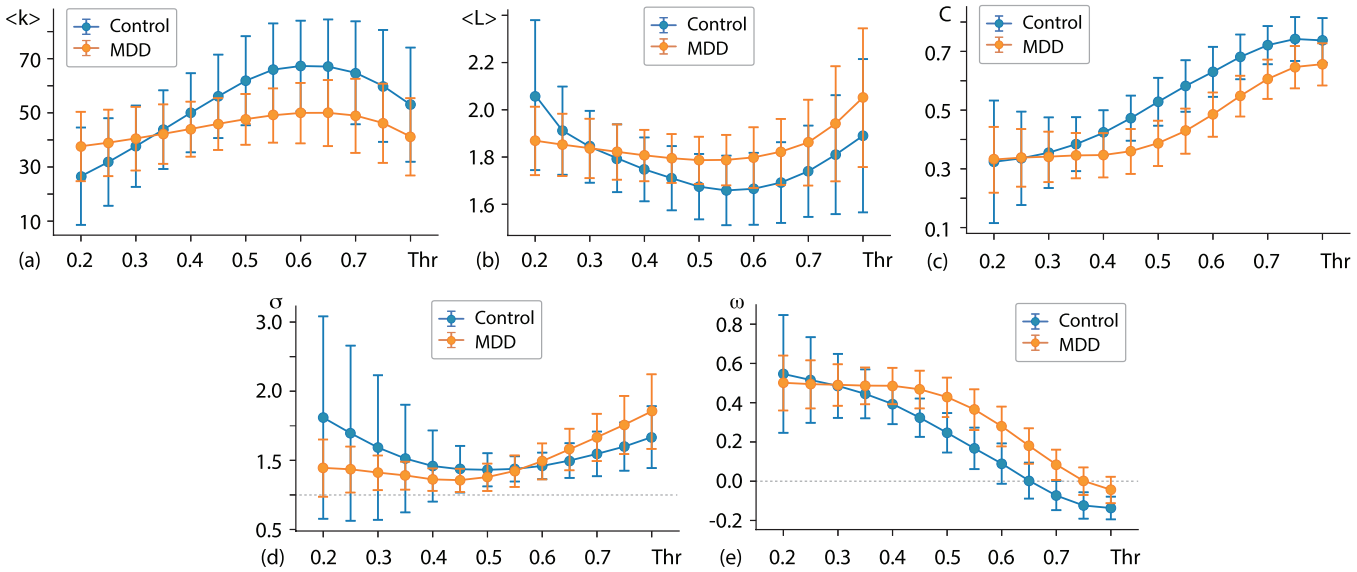

FIG. 5. The dependencies of the network measures on the threshold value *Thr* for HC (blue) and MDD (red) groups: (a) mean node degree $\langle k \rangle$, (b) average shortest path length $\langle L \rangle$, (c) clustering coefficient C, (d) small-world coefficient σ and (e) small-world measurement ω. Vertical lines correspond to standard deviation of the measure for the group. Horizontal dashed lines in (d) and (e) correspond to the reference values.

the dynamics of these parameters for the MDD group consensus network exhibit an opposite trend. Notably, for high threshold values, the linear regression parameters appear to be similar for both groups.

In contrast to the group-based network approach, the consensus network analysis reveals that only the degree distribution of the HC group can be well approximated in a linear fashion on a log–log scale, particularly for low threshold values. It is worth

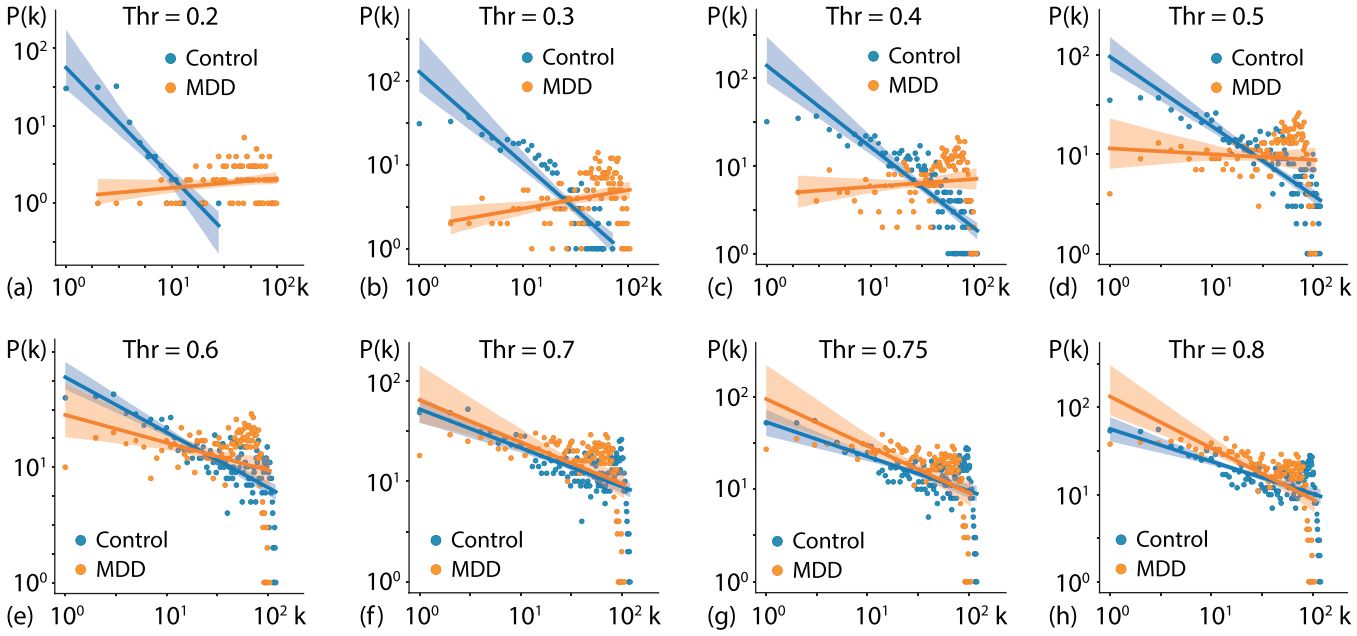

FIG. 6. Degree distributions of networks corresponding to each *Thr* value with linear regression: *Thr* = (a) 0.2, (b) 0.3, (c) 0.4, (d) 0.5, (e) 0.6, (f) 0.7, (g) 0.75, (h) = 0.8 for consensus networks. Each figure shows degree distributions for two groups of subjects (blue—MDD group, orange—control group).

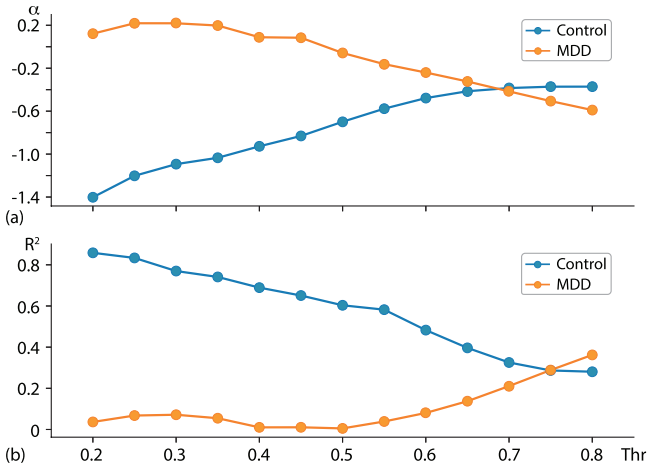

FIG. 7. The dependencies of the linear regression parameters on the threshold value *Thr* for control (blue) and MDD (red) groups: (a) the angle coefficient α and (b) the coefficient of determination R^2 for consensus networks.

noting that the angle coefficient α remains consistent between the two approaches, with a value of -1.4. Consequently, when employing the consensus network, we observe the characteristics of scale-free topology primarily for the HC group in relation to weak connections.

In the subsequent analysis, we computed five network measures: mean node degree $\langle k \rangle$, average shortest path length $\langle L \rangle$, clustering coefficient C, small-world coefficient σ, and small-world measurement ω. As depicted in Figs. 8(a)–8(d), the behavior of most measures exhibits significant differences between the two groups, with opposite changes observed. Specifically, for the HC group's consensus network at low threshold values, we observe a low node degree and clustering coefficient, accompanied by a high average shortest path length and small-world coefficient. Conversely, the MDD group's consensus network demonstrates a high node degree and clustering coefficient, as well as a low average shortest path length and small-world coefficient for the same range of threshold values. As the threshold value increases, the HC group's network exhibits an increase in the average node degree ($\langle k \rangle$) and clustering coefficient (C), while the average shortest path length ($\langle L \rangle$) and small-world coefficient (σ) decrease. In contrast, the MDD group's network demonstrates the opposite trend, eventually intersecting with the HC group at threshold values ranging from 0.3 to 0.5. Consequently, for high threshold values, both networks display inverse characteristics with respect to each other.

Particular attention should be given to the parameter ω due to its distinct dynamics compared to the other measures. Initially, the HC group's consensus network starts at a value of 1.0, while the MDD group's network begins at 0.4. As the threshold value *Thr* increases, both dependencies converge and decrease to approximately -0.2. Notably, the consensus network for the HC group transitions from a random topology ($\omega \approx 1.0$) to a small-world topology ($\omega \approx 0$) as the connection strengths change. On the other hand, the consensus network for the MDD group exhibits a topology that lies between fully random and small-world for weak connections. However, for high threshold values, it also transitions into a

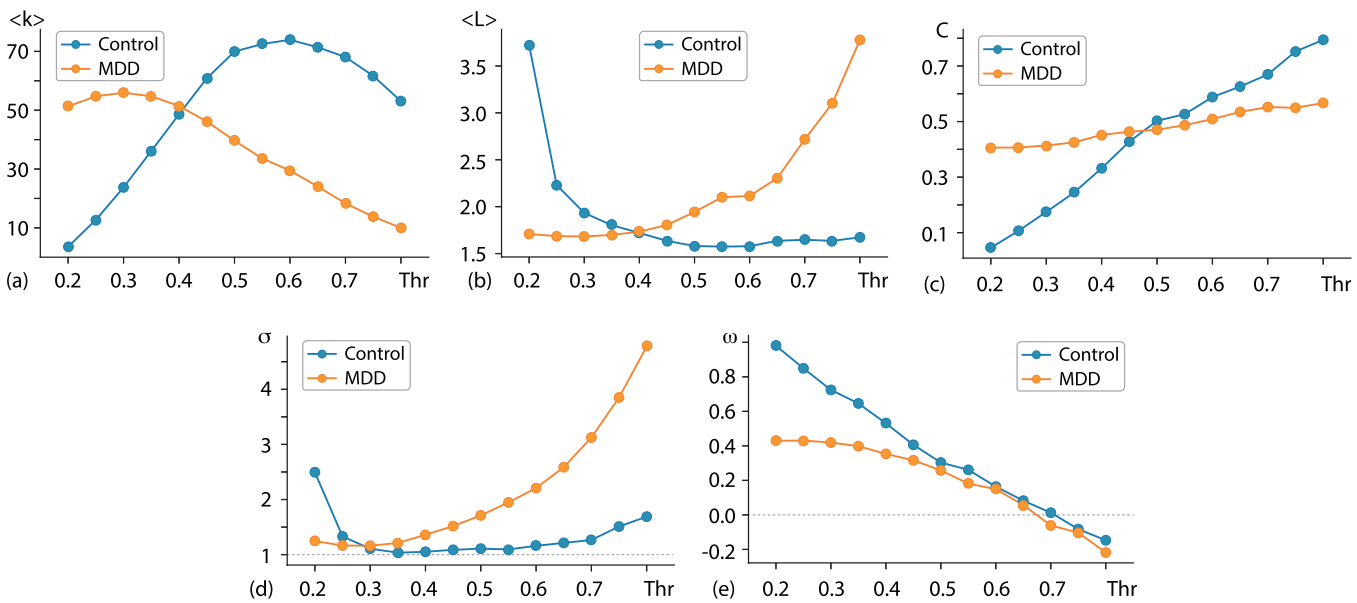

FIG. 8. The dependencies of the consensus network measures on the threshold value *Thr* for HC (blue) and MDD (red) groups: (a) mean node degree $\langle k \rangle$, (b) average shortest path length $\langle L \rangle$, (c) clustering coefficient C, (d) small-world coefficient σ and (e) small-world measurement ω. Horizontal dashed lines in (d) and (e) correspond to the reference values.

small-world topology, resembling the pattern observed in the HC group.

Thus, the analysis of consensus networks for healthy control and MDD subjects highlights distinct behaviors at different scales of coupling strength. These consensus networks uncover unique features of network topology that differ between the HC and MDD groups.

IV. CONCLUSION

In this study, we examined the functional connectivity networks of individuals with major depressive disorder (MDD) and healthy control (HC) groups using two different approaches. Firstly, we performed a group-based network analysis on the MDD patients and healthy control groups. Secondly, we analyzed the consensus networks specific to each group. For both approaches, we employed thresholding by retaining connections within a certain strength range ($Thr - \Delta Thr < w < Thr + \Delta Thr$ with $\Delta Thr = 0.2$). We then investigated the degree distributions using linear regression and calculated several network measures for each group, including mean node degree $\langle k \rangle$, average shortest path length $\langle L \rangle$, clustering coefficient C, small-world coefficient σ, and small-world measurement ω.

Our research using group-based network analysis revealed interesting findings regarding the network topology of both HC and MDD groups. As the threshold value increased, we observed a transition in the network topology from a scale-free-like structure to a combination of small-world and scale-free topologies for both groups. The degree distributions, particularly in the HC group, were well approximated by a linear function on a log–log scale, indicating a scale-free topology. Furthermore, the small-world measurement ω showed a transition from approximately 0.5 to nearly 0 as the threshold value increased, suggesting that the network topology in the presence of weak connections lies between fully random and small-world structures. As the threshold value increased, both groups exhibited a shift toward a small-world topology. Interestingly, the dynamics of all network characteristics remained consistent for both groups, posing challenges in using this approach for effective classification purposes.

Using the consensus network approach, we observed distinct behaviors of the consensus networks for both groups as the threshold value varied. In the case of the HC group, the degree distribution could be effectively approximated using linear regression on a log–log scale, but this was primarily observed for low threshold values. Interestingly, the consensus network for the HC group exhibited a transition in topology, shifting from a combination of scale-free and random topologies ($\omega \approx 1.0$) to a small-world topology ($\omega \approx 0$) as the connection strength changed. In contrast, the consensus network for the MDD group demonstrated a more complex behavior. For weak connections, the network topology was situated between fully random and small-world structures, and as the threshold value increased, it gradually transitioned into a small-world topology for strong connections. Hence, the consensus network for the HC group displayed a shift from a combination of scale-free and random topologies to a small-world topology with increasing threshold values, while the network topology for the MDD group exhibited uncertainty for weak connections and eventually converged toward a small-world topology for strong connections.

The utilization of the consensus network approach has provided valuable insights into the disparities between the HC and MDD groups in terms of consensus network measures across a wide range of threshold values. Notably, the mean node degree, average shortest path length, clustering coefficient, and small-world coefficient exhibited distinct and contrasting changes for the HC and MDD groups, intersecting at threshold values ranging from 0.3 to 0.5. These pronounced differences in the network measures present an opportunity for leveraging them in the classification of MDD patients, highlighting the potential of the consensus network approach for discerning between the two groups.

ACKNOWLEDGMENTS

The work was funded by the Russian Science Foundation (Grant No. 23-71-30010).

AUTHOR DECLARATIONS

Conflict of Interest

The authors have no conflicts to disclose.

Ethics Approval

Ethics approval for experiments reported in the submitted manuscript on animal or human subjects was granted. All participants provided written consent forms in accordance with the principles outlined in the Declaration of Helsinki. The study protocol received approval from the Ethical Committee of the Medical University of Plovdiv (Protocol 2/19 April 2018).

Author Contributions

Alexander N. Pisarchik: Conceptualization (equal); Formal analysis (equal); Methodology (equal); Writing – review & editing (equal). **Andrey V. Andreev:** Conceptualization (equal); Investigation (equal); Software (equal); Validation (equal); Visualization (equal); Writing – original draft (equal). **Semen A. Kurkin:** Conceptualization (equal); Formal analysis (equal); Investigation (equal); Methodology (equal); Writing – review & editing (equal). **Drozdstoy Stoyanov:** Data curation (equal); Investigation (equal); Writing – review & editing (equal). **Artem A. Badarin:** Formal analysis (equal); Software (equal); Validation (equal). **Rossitsa Paunova:** Data curation (equal); Investigation (equal); Resources (equal); Validation (equal). **Alexander E. Hramov:** Conceptualization (equal); Formal analysis (equal); Funding acquisition (equal); Methodology (equal); Supervision (equal); Writing – review & editing (equal).

DATA AVAILABILITY

The data that support the findings of this study are available from the corresponding author upon reasonable request.

REFERENCES

[1] D. S. Bassett and O. Sporns, "Network neuroscience," Nat. Neurosci. **20**(3), 353–364 (2017).

[2]A. E. Hramov, N. S. Frolov, V. A. Maksimenko, S. A. Kurkin, V. B. Kazantsev, and A. N. Pisarchik, "Functional networks of the brain: From connectivity restoration to dynamic integration," Phys.-Usp. **64**(6), 584 (2021).
[3]J. Wang, X. Zuo, and Y. He, "Graph-based network analysis of resting-state functional MRI," Front. Syst. Neurosci. **4**, 16 (2010).
[4]A. M. Bastos and J.-M. Schoffelen, "A tutorial review of functional connectivity analysis methods and their interpretational pitfalls," Front. Syst. Neurosci. **9**, 175 (2016).
[5]T. Yamada, R.-I. Hashimoto, N. Yahata, N. Ichikawa, Y. Yoshihara, Y. Okamoto, N. Kato, H. Takahashi, and M. Kawato, "Resting-state functional connectivity-based biomarkers and functional MRI-based neurofeedback for psychiatric disorders: A challenge for developing theranostic biomarkers," Int. J. Neuropsychopharmacol. **20**(10), 769–781 (2017).
[6]M. Perovnik, T. Rus, K. A. Schindlbeck, and D. Eidelberg, "Functional brain networks in the evaluation of patients with neurodegenerative disorders," Nat. Rev. Neurol. **19**(2), 73–90 (2023).
[7]D. Stoyanov, V. Khorev, R. Paunova, S. Kandilarova, D. Simeonova, A. Badarin, A. Hramov, and S. Kurkin, "Resting-state functional connectivity impairment in patients with major depressive episode," Int. J. Environ. Res. Public Health **19**(21), 14045 (2022).
[8]A. V. Andreev, S. A. Kurkin, D. Stoyanov, A. A. Badarin, R. Paunova, and A. E. Hramov, "Toward interpretability of machine learning methods for the classification of patients with major depressive disorder based on functional network measures," Chaos **33**(6), 063140 (2023).
[9]C. Giusti, R. Ghrist, and D. S. Bassett, "Two's company, three (or more) is a simplex: Algebraic-topological tools for understanding higher-order structure in neural data," J. Comput. Neurosci. **41**, 1–14 (2016).
[10]M. Zanin, P. Sousa, D. Papo, R. Bajo, J. García-Prieto, F. D. Pozo, E. Menasalvas, and S. Boccaletti, "Optimizing functional network representation of multivariate time series," Sci. Rep. **2**(1), 1–6 (2012).
[11]P. Zachar, D. S. Stoyanov, M. Aragona, and A. Jablensky, *Alternative Perspectives on Psychiatric Validation* (OUP, Oxford, 2014).
[12]E. N. Pitsik, V. A. Maximenko, S. A. Kurkin, A. P. Sergeev, D. Stoyanov, R. Paunova, S. Kandilarova, D. Simeonova, and A. E. Hramov, "The topology of fMRI-based networks defines the performance of a graph neural network for the classification of patients with major depressive disorder," Chaos, Solitons Fractals **167**, 113041 (2023).
[13]B. Holland and V. Moulton, "Consensus networks: A method for visualising incompatibilities in collections of trees," in *International Workshop on Algorithms in Bioinformatics* (Springer, 2003), pp. 165–176.
[14]M. Andjelković, B. Tadić, and R. Melnik, "The topology of higher-order complexes associated with brain hubs in human connectomes," Sci. Rep. **10**, 17320 (2020).
[15]A. Deeter, M. Dalman, J. Haddad, and Z.-H. Duan, "Inferring gene and protein interactions using pubmed citations and consensus Bayesian networks," PLoS One **12**(10), e0186004 (2017).
[16]B. R. Holland, K. T. Huber, V. Moulton, and P. J. Lockhart, "Using consensus networks to visualize contradictory evidence for species phylogeny," Mol. Biol. Evol. **21**(7), 1459–1461 (2004).
[17]M. Rubinov and O. Sporns, "Weight-conserving characterization of complex functional brain networks," NeuroImage **56**(4), 2068–2079 (2011).
[18]M. P. Van Den Heuvel, C. J. Stam, R. S. Kahn, and H. E. H. Pol, "Efficiency of functional brain networks and intellectual performance," J. Neurosci. **29**(23), 7619–7624 (2009).
[19]D. J. Watts and S. H. Strogatz, "Collective dynamics of 'small-world' networks," Nature **393**(6684), 440–442 (1998).
[20]G. Costantini and M. Perugini, "Generalization of clustering coefficients to signed correlation networks," PLoS One **9**(2), e88669 (2014).
[21]M. D. Humphries and K. Gurney, "Network 'small-world-ness': A quantitative method for determining canonical network equivalence," PLoS One **3**(4), e0002051 (2008).
[22]Q. Telesford, K. Joyce, S. Hayasaka, J. Burdette, and P. Laurienti, "The ubiquity of small-world networks," Brain Connect. **1**(5), 367–375 (2011).
[23]R. Albert and A.-L. Barabási, "Statistical mechanics of complex networks," Rev. Mod. Phys. **74**(1), 47 (2002).